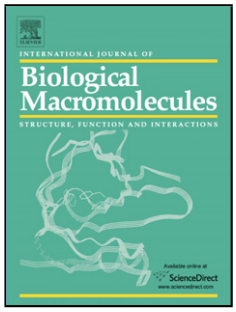

Title: Chitosan stabilized gold nanoparticle mediated self-assembled gliPnanobiosensor for diagnosis of Invasive Aspergillosis

Authors: Ira Bhatnagar, Kuldeep Mahato, Kranthi Kiran Reddy Ella, Amit Asthana, Pranjal Chandra

PII: S0141-8130(17)33790-X
DOI: https://doi.org/10.1016/j.ijbiomac.2017.12.084
Reference: BIOMAC 8746

To appear in: *International Journal of Biological Macromolecules*

Received date: 30-9-2017
Revised date: 20-11-2017
Accepted date: 13-12-2017

Please cite this article as: Ira Bhatnagar, Kuldeep Mahato, Kranthi Kiran Reddy Ella, Amit Asthana, Pranjal Chandra, Chitosan stabilized gold nanoparticle mediated self-assembled gliPnanobiosensor for diagnosis of Invasive Aspergillosis, International Journal of Biological Macromolecules https://doi.org/10.1016/j.ijbiomac.2017.12.084

Chitosan stabilized gold nanoparticle mediated self-assembled gliPnanobiosensor for diagnosis of Invasive Aspergillosis

Ira Bhatnagar[a*], Kuldeep Mahato[b], Kranthi Kiran Reddy Ella[c], Amit Asthana[a]

Pranjal Chandra[b*]

[a] *Clinical Research Facility,Medical Biotechnology Complex,CSIR - Centre for Cellular and Molecular Biology, Hyderabad-500007, India.*

[b] *Department of Biosciences and Bioengineering, Indian Institute of Technology Guwahati, Guwahati - 781039, Assam, India*

[c] *MNR Dental College & Hospital, Sangareddy, Telangana, India.*

[*] Corresponding authors
Dr. Ira Bhatnagar, Ph.D.
Clinical Research Facility, Medical Research Complex, CSIR - Centre for Cellular and Molecular Biology
Hyderabad-500007, India
Tel (Off.): +91-40-2719-5547
Email: ira@ccmb.res.in

Dr. Pranjal Chandra, Ph.D.
Department of Biosciences and Bioengineering
Indian Institute of Technology Guwahati, Guwahati - 781039, Assam, India.
Tel (Off.): +91-361-258-3207
Fax : +91-361-258-2249
Email : pchandra13@iitg.ernet.in

Abstract

Diagnosis of Invasive Aspergillosis (IA) casused by *Aspergillus fumigatus* in miniaturized setting is challenging with great importance in human health. In this direction, we have designed a sensitive electrochemical nanobiosensor for diagnosis of IA through detecting the virulent glip target gene (glip-T) in a miniaturized experimetal setting. The

sensor probe was fabricated based on 1,6-Hexanedithiol and chitosan stabilized gold nanoparticle mediated self-assembly of glip probes (glip-P) on gold electrode. It was characterized using *UV*-visible spectroscopy, cyclic voltametry and electrochemical impedance spectroscopy. The ability of the sensor to detect glip-T was analysed based on the hybridyzation reaction and the signal obtained using toluidine blue as indicator molecule. Analytical parameters were optimized in terms of glip-P concentration, temperature, reaction time, and concentration of toluidine blue. The biosensor showed the dynamic range between $1x10^{-14}$- $1x10^{-2}$ M with the detection limit of 0.32 ± 0.01 $x10^{-14}$(RSD < 5.2 %). The regeneration of biosensor was evaluated and the interference due to non-target oligonucleotide sequences was evaluated individualy as well as in mixed sample to validate the high selectivity of the designed sensor. The stability of the designed sensor was examined and practical applicability of biosensor was tested by detecting glip-T in real sample environment.

Keywords: Biosensors; medial diagnosis; invasive aspergillosis; gliP; gliotoxin, *Aspergillus fumigatus.*

1. Introduction

Invasive Aspergillosis (IA) caused by *Aspergillus* was first described as an opportunistic infection by Rankin in 1953[1] and remains the most common invasive mold infection worldwide [2]. The proliferation of IA starts when pathogenic encounters are not cleaned by the mucociliary clearances. The pathogens then infects the epithelial line of bronchioles and alveoli. Here, the primary defence against the pathogens is through the alveolar macrophages by killing the *Aspergillus* conidia, and recruitment of the neutrophils at the infection site. The evaded *Aspergillus* conidia from macrophages become the target to neutrophils' defence mechanism. The further survival of pathogen after this double layer

protection causes the symptoms of IA [3].The risk of developing this fatal clinical form of IA is higher in immunocompromised patients suffering from AIDS [4], neoplastic diseases, renal and bone marrow transplant recipients with corticotherapy. Although over 180 species are found within the genus *Aspergillus*, three species; *A. fumigatus*, *A. flavus*, and *A. terreus*, account for most cases of IA with *A. nidulans*, *A. niger*, and *A. ustus* being rare causes. It has been well documented that severe cases of IA are mediated through the production of a well-known secondary metabolite, Gliotoxin (GTX). The biosynthesis of GTX is also linked with gliP gene, a constituent of the GTX biosynthetic gene cluster [5].The enzyme encoded by the glip gene is directly involved in the production of GTX which in turn induces neutrophil apoptosis and thereby restricts the contribution of neutrophil host defence[3]. On the basis of these information, it is evident that glip gene can act as a genetic biomarker for detection of GTX producing *Aspergillus sp.*, which may eventually be helpful to diagnose IA. Determination of GTX production in IA patients is of utmost medical importance to determine the antifungal regime. In laboratory settings, polymerase chain reaction (PCR) based detections are used for the sensitive and rapid detection of any virulent gene [6]. The conventional microbiological tests are based on plate counting, membrane filtration, biochemical assessment, and spectrophotometry [7, 8]. These methods are trustworthy, but they need multistep processing, skilled professionals, and are not robust for point-of-care analysis. Essentially, these methods also lack miniaturization ability for quick and ultrafast detection of virulent genes.

The introduction of small, handy and robust volumes to such detections has been nowadays realized by using various biosensors [9, 10]. Over the years, biosensors have been designed to detect various type of analytes [11-15] including virulent genes [16, 17]. In order to obtain analytical signals for gene detection using any biosensor, various transducing systems have been adopted, such as; optical, chemiluminescence, fluorescence, and quartz

crystal microbalance [18].These systems lack in miniaturization diagnostics, have compromised detection limits, and importantly most of them have been applied for synthetic gene sequence analysis and not from the actual microbial species causing infection [19, 20]. Therefore, to address the real medical issues, a generic biosensor for quick detection of virulent genes directly from the microbial samples is very important and has clinical relevance. Compared to other transducing systems, an electrochemical transducing system is considered to be ultrafast and has great potential for point-of-care analysis [14, 21]. Therefore in the present study, we aim to develop an electrochemical biosensor for the detection of glip-T by DNA hybridization reaction for diagnosis of IA. To design a stable and ultrasensitive electrochemical biosensing method, an appropriate matrix is required to immobilize desired bio-molecules [18], followed by analysing the bio-molecular interactions which provide the analytical signal [17, 22]. The immobilization surface plays a vital role in biosensor fabrication in terms of signal transduction, stability, reproducibility, and regeneration [23]. Over the years bio-receptors have been immobilized on various matrices, such as; metallic electrodes, biopolymers, conducting polymers, nanomaterials, and self-assembled monolayers (SAM) [24]. Among all matrices, gold electrode(Au-E) is considered to be very unique due to its stability, highly conductive behaviour, and ability to form SAM with molecules having thiol groups (-SH) which offers a quick and highly sensitive sensor fabrication strategy [25, 26].

In the present study, an electrochemical biosensor has been fabricated by immobilizing glip-P onto chitosan stabilized gold nanoparticles (AuNPs) attached on 1,6-Hexanedithiol (HDT) SAM prepared on Au-E. The probe material /sensor probe was characterized using *UV*-visible spectroscopy, electrochemical impedance spectroscopy (EIS), and cyclic voltammetry (CV). The detection of glip-T was done by the hybridization reaction followed by intercalation of toluidine blue, which provided the analytical signal. The

analytical parameters for glip-T detection were then optimized and thereafter the detection limit of glip-T was determined in standard buffer as well as real sample matrix. Interference due to random nucleotides and non-target biochemicals was tested and regeneration of the designed biosensor was performed. To the best of our knowledge this is the first ever report where glip-T directly obtained from the fungal strain has been detected using a biosensor for diagnosis of IA.

2. Materials and methods

2.1.Chemicals and reagents

glip-P for glip-T gene sequences and other nontarget sequences were synthesized locally. Potassium ferricyanide ($C_6N_6FeK_3$), potassium ferrocyanide ($K_4Fe(CN)_6$), potassium phosphate monobasic (KH_2PO_4), potassium phosphate dibasic (K_2HPO_4), sodium chloride (NaCl), 1,6-Hexanedithiol ($HS(CH_2)_6SH$), 1% ethanolamine (C_2H_7NO), chitosan($(C_6H_{11}NO_4)_n$, mannose ($C_6H_{12}O_6$), β-glucans, potassium chloride (KCl),and toluidine blue ($C_{15}H_{16}N_3S^+$) were purchased from Sigma Aldrich (USA). Phosphate buffer of desired pH and strength was prepared using monobasic and dibasic sodium phosphates following a previously reported method [27]. For all the experiments, high grade de-ionized water (18.3 M Ω cm) and analytical grade chemicals were used at ambient temperature. Freshly prepared aqua-regia solution (HCl: HNO_3= 3:1) bath was used for cleaning laboratory glasswares followed by rinsing with de-ionized water. Piranha solution was prepared by mixing sulfuric acid (H_2SO_4) and hydrogen peroxide (H_2O_2) in the volumetric ratio of 3:1.

2.2. Sample preparation and validation: DNA extraction, PCR, and Gel electrophoresis

The pre-isolated (in our laboratory) *Aspergillus fumigatus* strain was inoculated in 10ml culture tubes of YPG medium containing Yeast (8% w/v), peptone (2% w/v), glycerol (1% v/v) and seawater: distilled water (3:2) at 37 ^oC temperature under 60% humid condition.

This 10ml of culture broth was used to inoculate culture flasks containing 1.0 Lt of YPG broth of similar composition. The inoculated culture flasks were incubated for a period of approximately seven days or until the top of the broth was covered with biomass/pellicle. The mycelia were frozen with liquid nitrogen then crushed in a mortar and pestle and stored at 4^{o}C. DNA was isolated from this frozen and crushed fungal biomass using fungal DNA isolation kit (Omega bio-tek, U.S.A. Catalogue no. D3390-01) as per manufacturer's instructions thereafter purity of DNA was determined through Nano drop instrument. This DNA was used as a template to amplify the glip-T gene segment using specific primers (glip forward- 5' GACCTCTGCCAGCTTTTTGA 3' and glip reverse- 5' GGATGATCGAAGATGTTGC 3') under optimized conditions and the amplified products of gene were verified by separating them in 1.5% agarose gel for 30 min at 100 V (figure not shown). For the biosensing analysis the PCR amplicons were quantified and detected using the designed biosensor.

2.3. Apparatus

The conventional three electrode system was used to perform the electrochemical analyses, where Ag/AgCl, platinum (Pt) wire, and modified Au-E were used as reference, counter, and working electrodes, respectively. The *UV*-vis spectrum was taken in the wavelength range between 300 and 800 (Perkin Elmer, Germany). All electrochemical experiments for biosensor characterization were performed in freshly prepared Zobell's solution [5mM$K_3Fe(CN)_6$, 6 mM $K_4Fe(CN)_6$, and 0.2 M KCl] using potentiostat/galvanostat, Kosentech, Mini-model (South Korea). Impedance spectra were recorded using EG&G Princeton Applied Research PARSTAT2263 at open circuit potential *vs.* Ag/AgCl using modulation amplitude of 10.0 mV between the frequency range of 0.10 Hz and 100 KHz.

2.4. Fabrication of biosensor probe

The step by step sensor development and the detection principle is shown in scheme 1. In the process of the biosensor development, Au-E was thoroughly cleaned by piranha solution followed by the sequential washing with 70% ethanol and distilled water for 2-3 min. This was followed by self-assembly of HDT on the previously cleaned Au-E to form Au-E/HDT surface. In the next step, the chitosan stabilized AuNPs were synthesized using a previously reported method [28] and self-assembled onto the Au-E/HDT electrode to form Au-E/HDT/AuNPs surface. Further, the thiolated glip-P was reacted with Au-E/HDT/AuNPs surface for an optimum time to get final sensing probe as Au-E/HDT/AuNPs/glip-P. The unbound probe was removed by multiple washing with TE buffer followed by reaction with 0.1 M mercaptoethanol for 1.0 min to remove any unbound glip-P probe. Next, the Au-E/HDT/AuNPs/glip-P sensor surface was treated with 1% ethanolamine prepared in 0.1 M PBS (pH 7.4) to block nonspecific cites in order to circumvent the false positive signals. The final designed probe was kept at room temperature until used.

Scheme 1 here

3.Results and Discussions.

3.1. Characterization of biosensor

At first the chitosan stabilized AuNPs were characterized using *UV* visible spectroscopy. A representative *UV* absorption spectra at 520 nm for the synthesized AuNPs was observed, indicating the successful formation of AuNPs (figure 1(A)), which was comparable with a previously reported result [28]. Next, the fabrications steps were confirmed by using EIS. Figure 1(B) shows the representative Nyquist plots for each layer of the sensing probe, where the bare Au-E shows Rct value of 2439 ± 68Ω (blue curve), which was increased after the self-assembly of HDT to 2831 ± 71 Ω (black curve). The increase in

the Rct value after HDT immobilization was most likely due to the insulating behaviour of HDT. After the self-assembly of chitosan stabilized AuNPs onto the Au-E/HDT layer, the Rct value significantly decreased to 1478 ± 54Ω (red curve) most likely due to increase in the conductivity of electrode surface due in presence of AuNPs. After the immobilization of thiolated glip-P on the Au-E/HDT/AuNPs electrode surface the Rct was increased to 4256 ± 172Ω (green curve), indicating the successful immobilization of glip-P.The increase in the Rct value after glip-P immobilization was due to the nonconducting behaviour of glip-P. All impedance data were analysed by a conventional Randle's equivalent circuit as shown in the inset of figure 1(B). The fabrication of biosensor development at each layer was also characterized by CV at a scan rate of 50 mVs^{-1} in 10 mM Zobell's solution (figure not shown). The current response due to ferricyanide/ferrocyanide redox process for Au-E/HDT surface decreased when compared to the bare Au-E electrode. A comparatively lower redox peak currents for Au-E/HDT surface were observed due to decrease in electron transfer after HDT immobilization. After successive immobilization of AuNPs, the redox peaks increased due to the rise in the conductivity of the electrode surface. We have also checked the redox behaviour of ferricyanide/ferrocyanide for electrode surface after glip-P immobilization. Here, the redox peak current significantly decreased as the resistance of electrode surface increased due to glip-P immobilization. The results obtained in EIS and CV complement each other which clearly indicates the successful fabrication of glip Biosensor.

Figure 1 here

3.2. Detection ability of Au-E/HDT/AuNPs/glip-P sensor probe

After validating the biosensor construction, we applied it to detect the glip-T in PCR product. For this purpose, the Au-E/HDT/AuNPs/glip-P sensor was incubated with the PCR amplicons for an optimum time at room temperature to form Au-E/HDT/AuNPs/glip-P/glip-T. After washing the sensor probe with 0.1 M PBS, it was treated with 1 x 10^{-5} M of toluidine

blue. Thereafter, the electrode was rinsed with 0.1 M PBS and CV was recorded by cyclic the potentials between 0.0 and -0.4 V *vs*. Ag/AgCl at a scan rate of 50.0 mVs^{-1}*v*s. Ag/AgCl in a deoxygenated 0.1 M PBS (pH 7.4). Figure 2 (A) shows characteristic CVs at Au-E/HDT/AuNPs/glip-P and Au-E/HDT/AuNPs/glip-P/glip-T after interacting with toluidine blue. A clear redox peak due to the direct electrochemical behaviour of toluidine blue was observed at -0.21/-0.23V *vs*. Ag/AgCl, which was most likely due its intercalation between the hybridized glip-P and glip-T (blue curve). To confirm that the redox signal was due to the interaction/hybridization between glip-P and glip-T, a control experiment was performed where Au-E/HDT/AuNPs/glip-P was allowed to react with toluidine blue in similar experimental conditions. Interestingly, negligible redox peak was observed ($p \leq 0.001$) in this case (reddotted curve), indicating that the redox peak in the earlier case was merely due to the successful interaction between Au-E/HDT/AuNPs/glip-P sensor probe and glip-T. To ensure the stability of the interaction betweenAu-E/HDT/AuNPs/glip-P sensor probe and glip-T, CVs were recorded at the scan rates between 20 and 100 mVs^{-1}(Figure 2 (B)). The peak currents were found to be directly related to the scan rates due to the surface-confined electrochemical process of intercalated toluidine blue, representing the stable interaction between Au-E/HDT/AuNPs/glip-P sensor probe and glip-T.These results clearly show that the designed Au-E/HDT/AuNPs/glip-P sensor probe is able to detect glip-T effectively.

Figure 2 here

3.3. Optimization of experimental parameters

In order to obtain high performance of the glip biosensor, various analytical parameters affecting the analytical signals were optimized. The experimental parameters for glip-T detection were optimized in terms of glip-P concentration, temperature, reaction time and concentration of toluidine blue at a constant glip-T concentration of $1x10^{-12}$ M (Figure3). The effect of glip-P concentration was studied between 10 and 90 ng mL^{-1}. The

pattern of analytical signals was found to be increased gradually from 10 to 70 ng mL^{-1}, however, no prominent increase over 70 ng mL^{-1} was observed possibly due to the complete coverage of the binding cites for glip-P immobilization (Figure 3(a)). Thus, concentration of 70 ng mL^{-1} glip-P was used in the subsequent experiments. The effect of temperature on the receptor target interaction was tested between 10 and 60^0C, where the signal did not increase between 10 and 20°C. Over 20°C the signal increased with increase in temperature till 40°C, while the current responses between 40 to 60°C were almost similar (Figure 3(b)). Thus, for the practical purpose, we performed successive experiments at 37°C. The reaction time between Au-E/HDT/AuNPs/glip-P sensor probe and glip-T was also studied between 2.0 and 30.0 mins (Figure 3(c)). The current response was increased on increasing reaction time from 2.0 to 20.0 mins, while over this time no significant increase in signal was observed. Based on this study an optimum 20.0 mins reaction time was applied in the subsequent experiments. The effect of toluidine blue concentration was tested in the range of 1 x 10^{-5}- 10 x 10^{-5}M (Figure 3(d)). The signal increased from 1x $10^{-5}$to 7x 10^{-5} M, however, above 7x 10^{-5}M toluidine blue concentration the signal did not increase significantly. Therefore, the toluidine blue concentration of 7x 10^{-5}M was used in further experiments.

Figure 3 here

3.4. Analytical performance of Au-E/HDT/AuNPs/glip-P sensor probe

The analytical performance of the developed Au-E/HDT/AuNPs/glip-P sensor was evaluated under the optimized experimental conditions. For this purpose, the developed Au-E/HDT/AuNPs/glip-P sensor probe was incubated with various concentrations of glip-T samples, followed by reaction with toluidine blue. After washing of electrode with 0.1 M PBS, differential pulse voltammograms (DPV) were recorded in the potentials ranging between 0.0 and -0.4 V *vs*. Ag/AgCl at a scan rate of 5.0 mVs^{-1}. Other associated

parameters were as follows: 0.1 V pulse amplitude, 2.0 ms sample width, 50.0 ms pulse width, and 1000.0 ms pulse period. Figure 4(A) shows the representative DPV curves with increasing concentrations of glip-T, where the current responses increase with increase in glip-T concentrations. The increase in current responses after binding with glip-T concentrations was most likely due to the increase in toluidine blue binding cites after glip-P and glip-T hybridization. Based on the obtained DPV signals, a calibration plot was obtained, which shows a linear dynamic range between $1x10^{-14}$ M and $1x10^{-2}$ M for glip-T detection (Figure 4(B)). The linear regression equation for the calibration plot is expressed as follows: ΔI (μA) = 29.213 (± 0.667) + 2.047 (± 0.057) [glip-T(M)] with the correlation coefficient of 0.995. The detection limit of glip-T was determined to be 0.32 ± 0.01 $x10^{-14}$ M (RSD < 5.2 %) based on the standard deviation of five times repeated measurements of the blank (95% confidence level, $n = 5$). This dose dependent analyses confirms that the developed biosensor is able to detect glip-T efficiently. The obtained detection limit, dynamic range, and detection time was lower or comparable to the recently reported genosensors (Table 1).We also corroborated our biosensing result by testing the interaction between glip-T and glip-P unmodified electrode surface modified electrode (*i.e.* Au-E/HDT/AuNPs surface) as a control experiment. No increase in the signals were obtained even at higher glip-T concentrations, validating that the signals obtained in former case were exclusively due to the interaction between Au-E/HDT/AuNPs/glip-P sensor probe and glip-T. This control experiment result clearly shows that no false positive signals are obtained while detecting glip-T using the designed biosensor.

Figure 4 and Table 1 here

3.5. Real sample experiment

The practical application of the designed biosensor was assessed by detecting glip-T in YPG medium added with various fungal cell components (eg: chitin, mannose, β-glucans) to create a mimicked real sample matrix. The real sample experiment was done by spike and recovery method [34], where the % recovery of glip-T from the real sample matrix was obtained using equation 1.

$$\% \text{ Recovery} = \frac{A - A'}{A''} X\ 100 \qquad \text{..... } \textit{Eq. (1)}$$

Here,(A) and (A') are the analytical response due to glip-T in the spiked and blank samples, respectively; (A'') is the analytical response of glip-T in the standard solutions. Figure 5(A) shows the comparative responses of glip-T detection in blank buffer (blue bars) as well as in the real sample matrix (green bars) between $1x10^{-14}$ M and $1x10^{-2}$ M, where a gradual increase in the signals were observed with increase in glip-T concentrations. The % recovery results show that glip biosensor is able to detect > 94.6% of target molecule from the real sample matrix, indicating that the developed biosensor can effectively detect glip-T in real sample matrix. This result also indicates that the real sample components do not interact with the sensing probe due to the fact that glip-P has no affinity towards these molecules. The linear regression equation for the calibration plot in the real sample is expressed as follows: ΔI (μA)=28.682 (±0.352)+1.983 (±0.039) [glip-T(M)] with the correlation coefficient of 0.961. The detection limit of glip-T in the real sample matrix was found to be $0.81 \pm 0.01\ x10^{-14}$ M (RSD <6.4 %) based on the standard deviation of five repeated measurements of the blank (95% confidence level, *n = 5*). A slightly higher glip-T detection limit (less sensitive) in the real sample was most likely due to the negligible matrix effect owing to components in the real sample environment.

Similar observation of relatively less sensitive detection in real sample matrix using biosensor has also been reported earlier [16].

3.6. Selectivity, reproducibility, and regeneration studies

Selectivity is considered to be one of the most important parameter to judge the practical applicability of any biosensor [14, 35]. Therefore, we did selectivity assay for Au-E/HDT/AuNPs/glip-P sensor against five random nucleotide sequences of similar length (mer) following the similar experimental conditions. The selectivity test was performed at 10^{-2}, 10^{-4}, 10^{-8} M concentrations of glip-T and non-target sequences. In all the five tested nucleotides, no signals were obtained indicating that the designed sensor doesn't interact with other nucleotide sequences, hence it is highly selective towards glip-T. The target glip-T may exist together with large pool of nucleotides in a real sample matrix, so we also performed mixed sample analysis by detecting glip-T in presence of five random sequences. Interestingly, the sensitivity for glip-T detection in such sample was found to be 93.6 ± 6.2 % (n = 5) as compared to when glip-T was detected distinctly. The obtained result confirms that the developed glip biosensor is highly specific and has the ability to detect target molecule in a mixed sample solution. Additionally, it is worthwhile to mention that in real sample the designed biosensor was able to detect glip-T in the presence of the chitin, mannose, β-glucans and YPG medium components with sensitivity. This also suggests that the biosensor is not only selective towards oligonucleotides, but also towards various other biochemicals.

The reproducibility of the glipbiosensor was examined which showed the RSD <4.7 % (n = 5) and under the analogous fabrication steps, while the electrode-to-electrode RSD was found to be <6.7 %. This insignificant variation in the signal was most likely due to the trivial variation in the biosensor development steps. We also studied the long term stability of the biosensor with respect to time. For this purpose, the sensor probe was kept in 0.1 M autoclaved PBS for several weeks until used. The sensor retained 95 ± 2 % sensitivity upto 7

weeks, while after 7 weeks the signal decreased ~ 9 ± 1 % which gradually decreased with time ($n = 5$). High stability was most likely due to the unique sensor design composed of only oligonucleotides as bioreceptors that are stable for long time compared to other protein based bioreceptors. Thus, the glip biosensor was practically stable up to 7 weeks which is directly related to the stable sensor fabrication and effective conjugation of the sensing components.

Biosensor regeneration is an important criteria for its commercial feasibility and cost effective diagnostics [36]. The regeneration ability of the designed Au-E/HDT/AuNPs/glip-P biosensor was performed by dipping the hybridized electrode (Au-E/HDT/AuNPs/glip-P/glip-T) in 25% urea, followed by multiple washing of the electrode surface with warm PBS. The result showed 100% ($n = 5$) regeneration even after third regeneration cycle, while the electrode retained ~90 % ($n = 5$) of the original signal upto seven regeneration cycles with a RSD of < 5.3 % (Figure 5(B)). The considerably good reusability of upto seven times was most likely due to the stability of the glip-P immobilized on to the metallic electrode which is devoid of thermally or chemically degradable molecules (*eg*: proteins, enzymes) in the sensing matrix.

Figure 5 here

4. Conclusions

A highly sensitive and selective biosensor has been designed for the diagnosis of Invasive Aspergillosis through detecting glip-T. The designed biosensor is systematically characterized by *UV*- visible spectroscopy, electrochemical impedance spectroscopy and voltammetry. The biosensor is able to detect the glip-T with an exceptional detection limit of 0.32 ± 0.01 $x10^{-14}$ M and 0.81 ± 0.01 $x10^{-14}$ M in standard buffer and real sample, respectively. The developed biosensor detects glip-T in merely ≤ 20 min, offering fast detection of IA causing and gliotoxin producing strains of *Aspergillus fumigatus*. The

sensor is also regenerated for seven times, indicating its reusability for cost effective diagnostics, which makes it a potential candidate for its translation into a miniaturized hand-held device for onsite glip-T detection from patients suffering from IA. Our analytical approach may help clinicians for fast IA diagnosis, which may eventually be helpful to design suitable therapeutic strategies for patients. The strategy described in the present study is easy, rapid, inexpensive, and generic, hence it can also be adopted for detection of other genetic biomarkers to facilitate a user friendly point-of-care detection module in hospitals and other related industries.

Acknowledgements: Dr. Pranjal Chandra acknowledges support from DST SERB (ECRA) Grant (ECR/2016/000100). K.M.acknowledges IIT Guwahati research fellowship.

References

[1] N.E. Rankin, Disseminated Aspergillosis and Moniliasis Associated with Agranulocytosis and Antibiotic Therapy. B.M. J. 1 (1953) 918-919.
[2] D.W. Denning, Invasive aspergillosis. Clin. Infect. Dis. (1998) 781-803.
[3] T.R.T. Dagenais, N.P. Keller, Pathogenesis of Aspergillus fumigatus in Invasive Aspergillosis. Clin. Microbiol. Rev. 22 (2009) 447-465.
[4] E. Mylonakis, T. Flanigan, J.D. Rich, T.F. Barlam, Pulmonary aspergillosis and invasive disease in AIDS. Chest 114 (1998) 251-262.
[5] D.M. Gardiner, B.J. Howlett, Bioinformatic and expression analysis of the putative gliotoxin biosynthetic gene cluster of Aspergillus fumigatus. FEMS microbiology letters 248 (2005) 241-248.
[6] J. Wilson, T. Hunt, Molecular Biology of the Cell: The Problems Book, 5th ed., Garland Publishing2007.
[7] G.D. Alderson, Microbiology: Experiments and Lab Techniques, 14 ed., Fountainhead Press2015.
[8] K.E. Al, Microbiology Experiments: A Health Science Perspective, McGraw Hill Educaton 2016.
[9] P. Chandra, H.-B. Noh, R. Pallela, Y.-B. Shim, Ultrasensitive detection of drug resistant cancer cells in biological matrixes using an amperometric nanobiosensor. Biosens. Bioelectron. 70 (2015) 418-425.
[10] P. Chandra, H.-B. Noh, M.-S. Won, Y.-B. Shim, Detection of daunomycin using phosphatidylserine and aptamer co-immobilized on Au nanoparticles deposited conducting polymer. Biosens. Bioelectron. 26 (2011) 4442-4449.
[11] A. Kumar, A. Hens, R.K. Arun, M. Chatterjee, K. Mahato, K. Layek, N. Chanda, A paper based microfluidic device for easy detection of uric acid using positively charged gold nanoparticles. Analyst 140 (2015) 1817-1821.
[12] S. Chung, P. Chandra, J.P. Koo, Y.-B. Shim, Development of a bifunctional nanobiosensor for screening and detection of chemokine ligand in colorectal cancer cell line. Biosens. Bioelectron. 100 (2018) 396-403.
[13] K. Mahato, A. Srivastava, P. Chandra, Paper based diagnostics for personalized health care: Emerging technologies and commercial aspects. Biosens. Bioelectron. 96 (2017) 246-259.
[14] K. Mahato, A. Kumar, P. Kumar Maurya, P. Chandra, Shifting paradigm of cancer diagnoses in clinically relevant samples based on miniaturized electrochemical nanobiosensors and microfluidic devices. Biosens. Bioelectron. (2017).
[15] H.-B. Noh, P. Chandra, Y.-J. Kim, Y.-B. Shim, A Simple Separation Method with a Microfluidic Channel Based on Alternating Current Potential Modulation. Anal. Chem. 84 (2012) 9738-9744.
[16] Kashish, S. Bansal, A. Jyoti, K. Mahato, P. Chandra, R. Prakash, Highly Sensitive In Vitro Biosensor for Enterotoxigenic Escherichia coli Detection Based on ssDNA Anchored on PtNPs-Chitosan Nanocomposite. Electroanalysis.
[17] P. Chandra, Y.N. Tan, S.P. Singh, Next Generation Point-of-care Biomedical Sensors Technologies for Cancer Diagnosis, 1 ed.2017.
[18] P. Chandra, Nanobiosensors for personalized and onsite biomedical diagnosis, The Institution of Engineering and Technology2016.
[19] S.H. Qaddare, A. Salimi, Amplified fluorescent sensing of DNA using luminescent carbon dots and AuNPs/GO as a sensing platform: A novel coupling of FRET and DNA hybridization for homogeneous HIV-1 gene detection at femtomolar level. Biosens. Bioelectron. 89 (2017) 773-780.
[20] C. Chan, J. Shi, Y. Fan, M. Yang, A microfluidic flow-through chip integrated with reduced graphene oxide transistor for influenza virus gene detection. Sens. Actuat. B: Chem. (2017).
[21] R. Pallela, P. Chandra, H.-B. Noh, Y.-B. Shim, An amperometric nanobiosensor using a biocompatible conjugate for early detection of metastatic cancer cells in biological fluid. Biosens. Bioelectron. 85 (2016) 883-890.

[22] M.A. Rahman, P. Kumar, D.-S. Park, Y.-B. Shim, Electrochemical sensors based on organic conjugated polymers. Sensors 8 (2008) 118-141.
[23] J.D. Newman, A.P. Turner, Biosensors: principles and practice. Essays in Biochemistry 27 (1992) 147-159.
[24] A.P. Turner, Biosensors: sense and sensibility. Chem. Soc. Rev. 42 (2013) 3184-3196.
[25] Y. Xue, X. Li, H. Li, W. Zhang, Quantifying thiol-gold interactions towards the efficient strength control. Nat. Commun. 5 (2014) 4348.
[26] M. Choudhary, P. Yadav, A. Singh, S. Kaur, J. Ramirez-Vick, P. Chandra, K. Arora, S.P. Singh, CD 59 targeted ultrasensitive electrochemical immunosensor for fast and noninvasive diagnosis of oral cancer. Electroanalysis 28 (2016) 2565-2574.
[27] Y. Zhu, P. Chandra, C. Ban, Y.-B. Shim, Electrochemical Evaluation of Binding Affinity for Aptamer Selection Using the Microarray Chip. Electroanalysis 24 (2012) 1057-1064.
[28] H. Huang, X. Yang, Synthesis of Chitosan-Stabilized Gold Nanoparticles in the Absence/Presence of Tripolyphosphate. Biomacromolecules 5 (2004) 2340-2346.
[29] S. Sedighi-Khavidak, M. Mazloum-Ardakani, M. Rabbani Khorasgani, G. Emtiazi, L. Hosseinzadeh, Detection of aflD gene in contaminated pistachio with Aspergillus flavus by DNA based electrochemical biosensor. Int. J. Food Properties (2017) 1-12.
[30] S. Siddiquee, N.A. Yusof, A.B. Salleh, F.A. Bakar, L.Y. Heng, Electrochemical DNA biosensor for the detection of specific gene related to Trichoderma harzianum species. Bioelectrochemistry 79 (2010) 31-36.
[31] M. Tak, V. Gupta, M. Tomar, Flower-like ZnO nanostructure based electrochemical DNA biosensor for bacterial meningitis detection. Biosens. Bioelectron. 59 (2014) 200-207.
[32] M.H. Abdalhai, A.M. Fernandes, X. Xia, A. Musa, J. Ji, X. Sun, Electrochemical Genosensor To Detect Pathogenic Bacteria (Escherichia coli O157:H7) As Applied in Real Food Samples (Fresh Beef) To Improve Food Safety and Quality Control. J. Agric. Food Chem. 63 (2015) 5017-5025.
[33] X. Qi, H. Gao, Y. Zhang, X. Wang, Y. Chen, W. Sun, Electrochemical DNA biosensor with chitosan-Co3O4 nanorod-graphene composite for the sensitive detection of staphylococcus aureus nuc gene sequence. Bioelectrochemistry 88 (2012) 42-47.
[34] S. Verma, A. Singh, A. Shukla, J. Kaswan, K. Arora, J. Ramirez-Vick, P. Singh, S.P. Singh, Anti-IL8/AuNPs-rGO/ITO as an Immunosensing Platform for Noninvasive Electrochemical Detection of Oral Cancer. ACS Appl. Mater. Interfaces 9 (2017) 27462-27474.
[35] A. Paziewska−Nowak, J. Jankowska−Śliwińska, M. Dawgul, D.G. Pijanowska, Selective Electrochemical Detection of Pirarubicin by Means of DNA-modified Graphite Biosensor. Electroanalysis 29 (2017) 1810-1819.
[36] W.C.A. Koh, P. Chandra, D.-M. Kim, Y.-B. Shim, Electropolymerized self-assembled layer on gold nanoparticles: detection of inducible nitric oxide synthase in neuronal cell culture. Anal. Chem. 83 (2011) 6177-6183.

Figure captions:

Figure 1. (A) *UV*-visible spectra of chitosan stabilized AuNPs and (B) Nyquist plots for glip biosensor characterization for Au-E, Au-E/HDT, Au-E/HDT/AuNPs, Au-E/HDT/AuNPs/glip-P surfaces, inset shows the simple Randle's circuit used for data fitting.

Figure 2.(A) CVs for Au-E/HDT/AuNPs/glip-P (red dotted curve) andAu-E/HDT/AuNPs/glip-P/glip-T(blue curve) after interacting with toluidine blue, (B) Plots of the redox peak currents*vs.* scanrates for Au-E/HDT/AuNPs/glip-P/glip-T interacted with toluidine blue.

Figure 3. Optimization of experimental parameters (a) glip-P concentration, (b) temperature, (c) reaction time, and (d) toluidine blue concentration.

Figure 4. (A) DPV curves with increase in glip-T concentrations between $1x10^{-14}$ M (i) and $1x10^{-2}$M (vii) in deoxygenated 0.1 M PBS and (B) the calibration plot based on the obtained DPV signals.

Figure 5.(A) Comparative dose dependent detection of glip-T in buffer (blue) and real sample (green), and (B) histograms showing the regeneration of Au-E/HDT/AuNPs/glip-P biosensor.

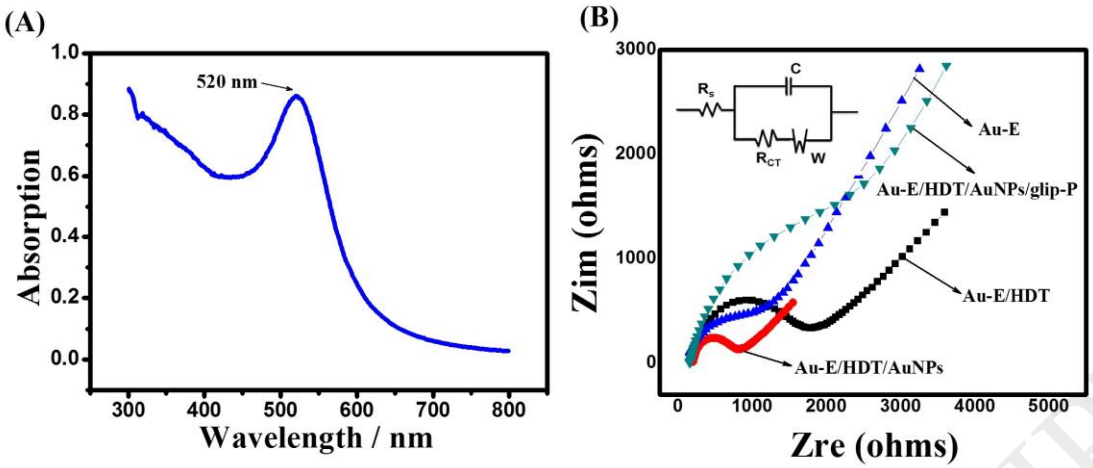

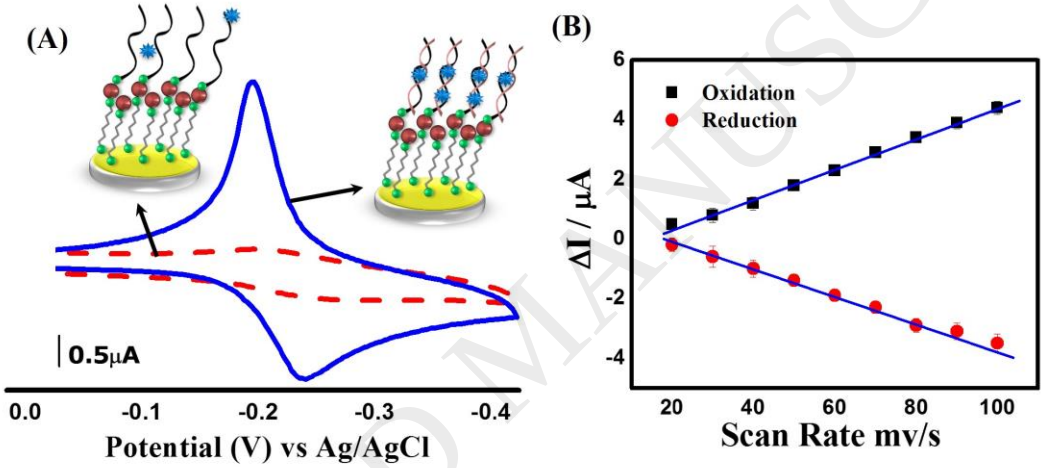

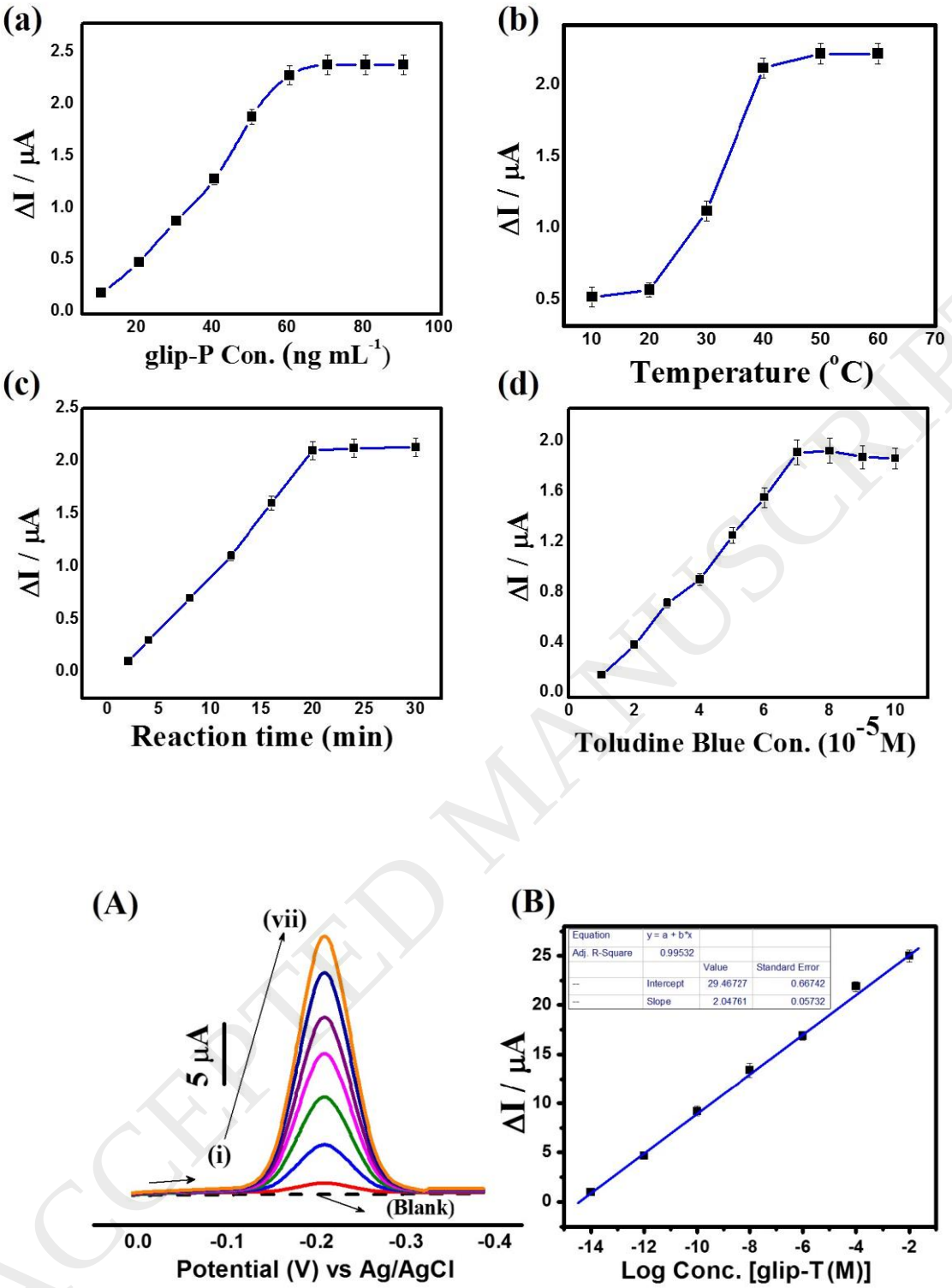

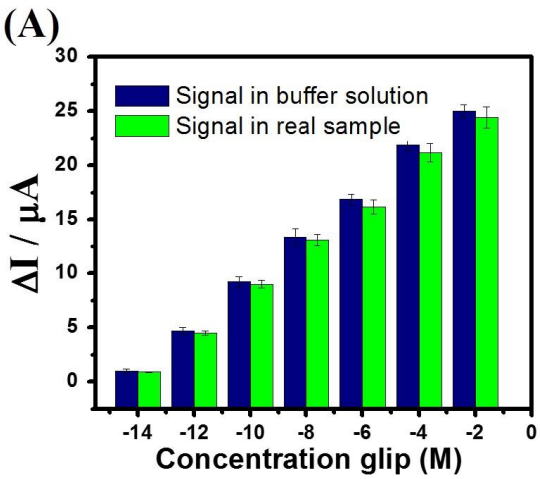

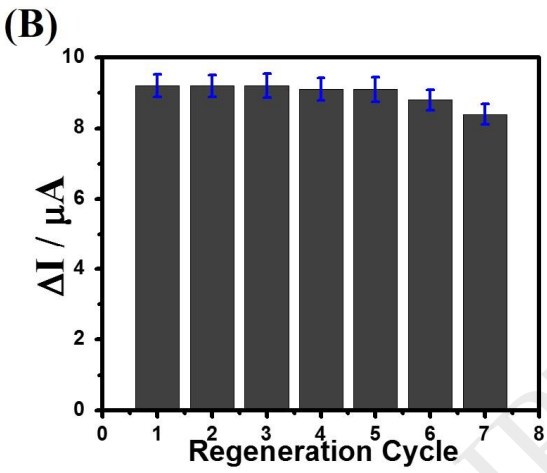

Scheme caption

Scheme 1. Detailed illustration of glip biosensor fabrication and detection principle.

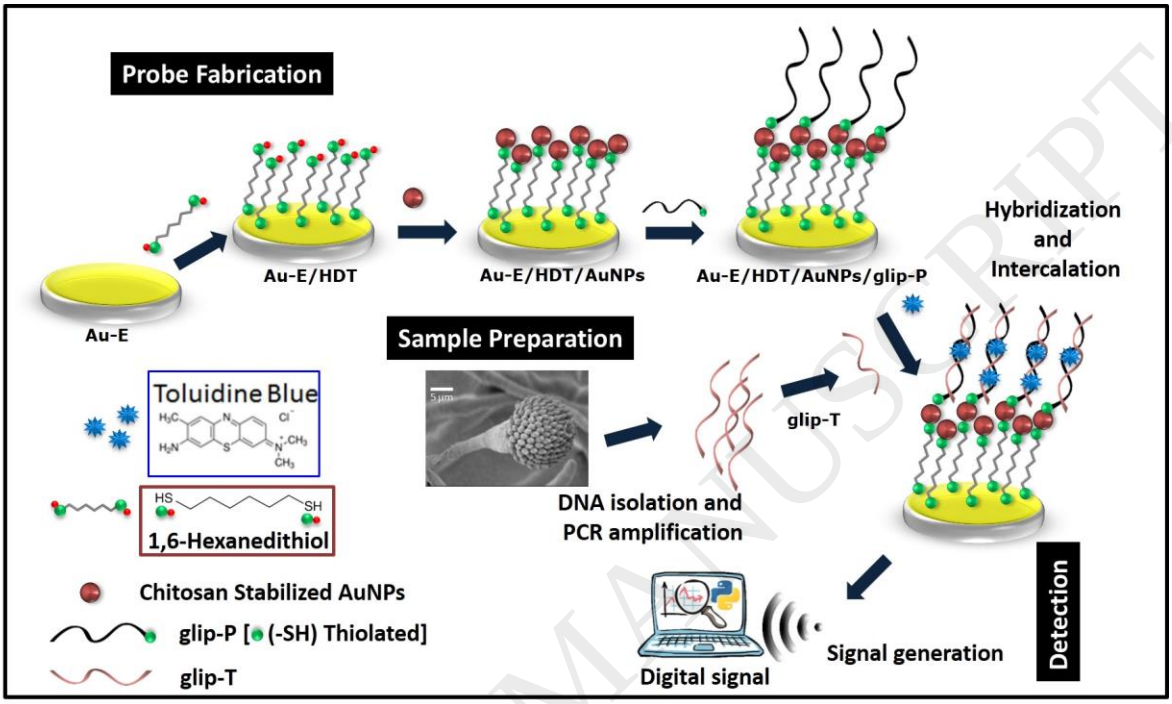

Table 1: Comparative analysis of glip biosensor with various other genosensors. *NR: Not Reported*

Transducing surface	Analyte	Dynamic Range	Detection Limit	Real Sample	Detection Technique(s)	Detection Time	Reference
ssDNA/AuNP/GCE	aflD gene	1 nM - 10 µM	0.55 nM	Infected Pistachio	Electrochemical Impedance Spectroscopy	240 min	[29]
ssDNA/SAM/MPA/AuE	Gene sequence of *Trichoderma harzianum*	1–20 ppm	NR	NR	Voltammetry	60 min	[30]
ss (th)-DNA/ZNF/Pt/Si	ctrA gene	5-240 ng/µl	5 ng/µl	NR	Electrochemical Impedance Spectroscopy	NR	[31]
$ssDNA^P$/chitosan /PtNPs-SPCE	Enterotoxigenic *Escherichia coli (ST gene)*	1×10^{-12} M-1×10^{-4} M	3.6×10^{-14} M	Surface water	Electrochemical Impedance Spectroscopy	≤ 20 min	[16]
ssDNA/PAMAM/Cys/ AuE	*Streptococcus pyogenes*	10^{-3} - 10^{-1} ng/6 µL	130 fg/6 µL	Throat swab	Amperometry and Differential Pulse Voltammetry	< 30 min	[17]
ssDNA/CdSNPs/tDNA/fDNA/MWCNT-Chi-Bi/GCE	*Escherichia coli* O157:H7	1.94×10^{-13} - 2.01×10^{-14} M	1.97×10^{-14} M	Fresh beef meat	Electrochemical Impedance Spectroscopy	NR	[32]
ssDNA/Chi–Co_3O_4–GR/CILE	*Staphylococcus aureus* (nuc gene)	1.0×10^{-12} - 1.0×10^{-6} M	4.3×10^{-13} M	NR	Differential pulse voltammetry	NR	[33]

ssDNA (glip-P) / AuNPs / HDT/AuE	*Aspergillus fumigatus* (glip-T)	$1x10^{-14}$- $1x10^{-2}$ M	0.32 ± 0.01 $x10^{-14}$ M	Fungal component mixture	Differential pulse voltammetry	< 20 min	Present work